# Effects of Graphene Modification on the Bioactivation of Polyethylene-Terephthalate-Based Artificial Ligaments

Chun-Hui Wang,[†,§] Zhong-Shang Guo,[†,§] Fei Pang,[‡] Li-Yuan Zhang,[‡] Ming Yan,[†] Jin-Hong Yan,[†] Ke-Wen Li,[†] Xiao-Jie Li,[†] Yong Li,[†] Long Bi,*,[†] and Yi-Sheng Han*,[†]

[†]Department of Orthopaedics, Xijing Hospital, Fourth Military Medical University, No. 15 West Change Road, Xi'an 710032, China
[‡]Department of Physics, Renmin University of China, No. 59 Zhongguancun Street, Beijing 100872, China

Ⓢ Supporting Information

**ABSTRACT:** The objective of this study was to investigate whether surface coating with graphene could enhance the surface bioactivation of PET-based artificial ligaments to accelerate graft-to-bone healing after anterior cruciate ligament reconstruction. In an in vitro study, the proliferation of MC3T3-E1 cells and their differentiation on the scaffolds were quantified via 3-(4,5-dimethylthiazol-2-yl)-2,5-diphenyltetrazolium bromide and real-time polymerase chain reaction assays. The significantly higher optical-density values and transcription levels of osteoblast-specific genes indicated that graphene modification could promote the proliferation of MC3T3-E1 cells and accelerate their specific differentiation into osteogenic lineages on scaffolds. In an in vivo test, rabbits were used to establish an extra-articular graft-to-bone healing model. At 4, 8, and 12 weeks after surgery, biomechanical tests, microcomputed tomography analysis, and histological observations were performed. The final results demonstrated that the microstructural parameters, the average mineral apposition rate of the bone, and the biomechanical properties of the graphene-coated polyethylene terephthalate (PET)-based artificial ligament (G-PET-AL) group were significantly higher than those of the PET-AL graft group ($P < 0.05$). The results of Van Gieson staining indicated that in the G-PET-AL group, there was more newly formed bone than there was in the group in which nongraphene-coated PET-ALs were used. In conclusion, graphene exhibits considerable potential for enhancing the surface bioactivation of materials.

**KEYWORDS:** graphene, surface modification, polyethylene terephthalate, artificial ligament, bioactivity, graft-to-bone healing
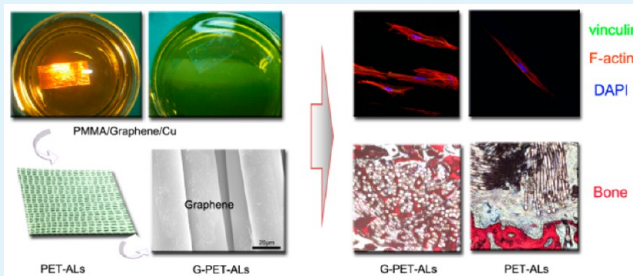
## 1. INTRODUCTION

Anterior cruciate ligament (ACL) rupture is a common injury of the articular ligaments,[1] especially for young, athletic, active individuals in the 16−39-year age group,[2,3] because of the poor self-healing ability of a ruptured ACL. ACL reconstruction is the most common method of restoring the stability of the injured knee joint.[4,5] In the United States, the incidence of ACL surgery is 91 per 100,000 individuals.[6] The incidence in China is approximately 3- to 5-fold greater. Both autologous and allogeneic grafts are traditionally used for ACL reconstruction. However, the disadvantages of this approach include donor-site morbidity, a long rehabilitation period, and early osteoarthritic changes. Because of theoretical advantages such as abundant strength, immediate load support, and reduced postoperative rehabilitation, artificial ligaments have increased in popularity since the 1980s.[7−9] In particularly widespread use is the Ligament Advanced Reinforcement System (LARS) ligament, composed of polyethylene terephthalate (PET), which was developed by a French surgeon, Dr. J.P. Laboureau, in 1992.[10,11] PET's biomechanical properties of resistance to tension, flexion, and torsion load can reduce friction and avoid tunnel enlargement.[12−14] Nevertheless, the low surface energy

of PET makes it difficult for cells to adhere and encapsulate on PET fibers. Successful repair depends on the establishment of a permanent and stable conjunction between the artificial ACL and the host tissues. To overcome the disadvantages of the biological inertness of PET and improve the interactions between PET and host tissues, surface modification of the PET should be performed.[13,15]

Several modification methods have been introduced to improve the surfaces of PET materials to promote the survival, attachment, and proliferation of seeding cells as well as their directed differentiation.[14] Nevertheless, certain drawbacks, such as potential pathogenic infections, low availability, the high cost and difficult storage of active proteins such as growth factors[16,17] and bioactive proteins,[18] and the negative effects of certain techniques such as laser modification, bioceramic coating, and radiation grafting would reduce the strength, porosity, and toughness of PET, which would restrict the application of surface modification.[19−21] Because it consists of

only a single layer of carbon atoms and possesses the excellent material properties of small thickness, large surface area, low mass density, and the highest Young's modulus (0.5−1 TPa) of any known material,[22] graphene has promise as a possible modifying agent for the surface modification of PET.[23,24] In the field of biomedical applications, graphene has been used for cellular imaging, drug delivery, and cooperative therapeutic agents for tumor cells.[25,26] Studies have demonstrated that graphene can accelerate the differentiation of human mesenchymal stem cells (hMSCs) into osteogenic lineages and the differentiation of human neural stem cells into neurons.[24,27,28] However, it remains unknown whether graphene can be transferred onto the surface of PET, the most commonly used material for artificial ligaments, to improve the bioactivity of the PET and thereby enhance the adhesion, proliferation, and differentiation of seeding cells thereon.

The objective of this study was to modify PET-based artificial ligaments (PET-ALs) by transferring graphene onto these ligaments on a large scale and observing the effects of the graphene on the bioactivation of the PET-ALs. We hypothesize that the outstanding surface activity and electrical conductivity of graphene should improve the attachment and proliferation of cells as well as their differentiation into osteogenic lineages, thus promoting graft-to-bone healing.

## 2. MATERIALS AND METHODS

### 2.1. Preparation of PET-ALs and Graphene-Coated PET-ALs (G-PET-ALs).
The PET-ALs were fabricated from high-purity PET fibers (90% crystalline) using an independent improvement Raschel warp knitting machine (ML35C Germany KarlMayer). The horizontal density (Pa) and longitudinal density (Pb) were 20/5 cm and 40/5 cm, respectively, and the machine speed was 600 r/min. PET sheets (5 cm × 5 cm) were cut from the braided PET-ALs, immersed in absolute ethanol for 24 h, and washed with an ultrasonic cleaner for 20 min to remove dirt.

We grew graphene on copper foils (25 $\mu$m thick) at temperatures of up to 1000 °C using a mixture of methane and hydrogen under an argon atmosphere ($CH_4/H_2/Ar$ = 50:60:200 standard cubic centimeters per minute) via chemical vapor deposition (CVD).[29,30] After a poly(methyl methacrylate) (PMMA) layer was coated onto the copper/graphene surface, we etched the copper foil using an $FeCl_3$ solution, and we then placed the free-standing PMMA/graphene membrane onto the PET-AL (with the graphene facing the surface of the PET-AL).[31] Finally, we obtained graphene-coated PET-ALs (G-PET-ALs) by using acetone to dissolve the PMMA, washing each sample several times with absolute ethanol, rinsing it with deionized water, and then drying it in a drying oven at 60 °C for 24 h.

### 2.2. Graft Characterization.
*2.2.1. Scanning Electron Microscopy (SEM).* The morphologies of the PET-ALs and G-PET-ALs were evaluated using a scanning electron microscope (HITACHI-S4800, Japan) at a voltage of 5 kV.

*2.2.2. Raman Spectroscopy Analysis.* The fine structures of graphene on the copper, PET-ALs, and G-PET-ALs were characterized via Raman spectroscopy (HORIBA JOBIN YVON -HR800, Japan) using a laser at a wavelength of 633 nm.

*2.2.3. Porosity.* The open porosity of the four types of PET-ALs was evaluated based on the principle of liquid displacement[34] ($n$ = 6). The following equation was used to calculate the porosity of the PET-ALs:

$$\varphi\ (\%) = \frac{[(P_T - P_S) - (P_R - P_P)]/\rho_{hex}}{V_N - (P_R - P_P)/\rho_{hex}} \times 100$$

where $P_T$ is the weight of the pycnometer when completely filled with hexane and the tested PET-ALs; $P_S$ is the weight of the dried pycnometer and the tested PET-ALs; $P_R$ is the weight of the pycnometer and the residual hexane after the removal of the tested PET-ALs; $P_P$ is the weight of the dried pycnometer; $V_N$ is the nominal volume of the pycnometer ($V_N$ = 50 mL); and $\rho_{hex}$ is the density of hexane at the measurement temperature.

*2.2.4. Wettability Properties.* The wettability of the PET-ALs and G-PET-ALs was evaluated via static contact-angle measurements at three different locations on each sample ($n$ = 6). A water drop of 3 $\mu$L in volume was placed on the surface of each PET-AL and G-PET-AL. In that moment, photographs were captured using a side-view microscope connected to a camera (Nikon, USA). The contact angle was calculated by applying a spherical approximation using ImageJ 1.48 software, and each value was obtained as the mean of 18 measurements.

*2.2.5. Mechanical Properties.* The PET-ALs and G-PET-ALs ($n$ = 6) were rolled up to 60 mm in length and 4.0 mm in diameter and were tested under tension using an Instron testing system (Model 4442, 10kN, Instron Inc., MA) at an elongation rate of 10 mm/min. The load−deformation curve was recorded, from which the ultimate failure load (N) was measured. Stiffness (N/mm) was calculated from the slope of the linear region of the load−deformation curve at the maximal load-to-failure point.

### 2.3. In Vitro Tests.
*2.3.1. Cell Culture and Seeding.* The MC3T3-E1 murine osteoblastic cell line (Riken Cell Bank) was used for in vitro experiments. The cells were cultured in $\alpha$-MEM medium (Corning, USA) with 10% fetal bovine serum (FBS, Gibco, USA), 100 U/mL penicillin, and 100 U/mL streptomycin (Sigma) at 37 °C in a humidified atmosphere that contained 5% $CO_2$ and 95% air.

G-PET-AL scaffold sheets as well as stainless PET- AL sheets as the control (35 mm in diameter) were sterilized with cobalt-60 (Irradiation dose: 20kGy); then, the sheets were transferred into a nontreated six-well plate. Cells in the logarithmic phase were seeded at the density of 1× 10⁵ cells/well in the six-well plate. The sheets were transferred into another nontreated six-well plate after 1 day of culturing time. The medium was exchanged every 2 days for a period up to 7 days.

*2.3.2. Cell Attachment and Proliferation in Vitro.* The attachment and proliferation of the MC3T3-E1 cells on the PET-ALs and G-PET-ALs were investigated. The cell-attachment morphologies were monitored via SEM (HITACHI-S4800, Japan) after the cells had been seeded and cultured for 1 day and 5 days ($n$ = 3). At each time point, the sheets were gently washed three times with phosphate-buffered saline (PBS) and fixed overnight in 2.5% glutaral solution, then washed three times with DDW (doubly distilled water). Prior to SEM analysis, the sheets were dehydrated through a series of ethanol dilutions (20, 40, 60, 80, and 100%, 10 min each). The samples were sputter coated with gold and examined via SEM at an accelerating voltage of 5 kV. Cell proliferation on the sheets ($n$ = 6) was quantified via an 3-(4,5-dimethylthiazol-2-yl)-2,5-diphenyltetrazolium bromide (MTT, Sigma) assay after 1, 3, 5, and 7 days of culturing time. At each time point, we transferred the sheets into another nontreated six-well plate, added 2 mL of new medium and 200 $\mu$L of 5 mg/mL MTT solution, and cultured the plate in an incubator at 37 °C with

**Table 1. Primers Used for RT-PCR Validation**

| genes | forward primer sequences (5′−3′) | reverse primer sequences (5′−3′) |
|---|---|---|
| GAPDH | TGCTGGTGCTGAGTATGTGGT | AGTCTTCTGGGTGGCAGTGAT |
| COL1A1 | GACATGTTCAGCTTTGTGGACCTC | GGGACCCTTAGGCCATTGTGTA |
| RUNX2 | GAACCAAGAAGGCACAGACAGA | GGCGGGACACCTACTCTCATAC |
| OPN | TACGACCATGAGATTGGCAGTGA | TATAGGATCTGGGTGCAGGCTGTAA |
| OCN | ACCATCTTTCTGCTCACTCTGCT | CCTTATTGCCCTCCTGCTTG |

5% $CO_2$ for 4 h. Thereafter, the medium was removed, 1 mL of dimethyl sulfoxide (DMSO, Sigma) was added to each well, and the plate was vibrated using a micro-oscillator at 1500 rpm for 10 min; then, 120 $\mu$L of the DMSO was withdrawn and placed into a 96-well plate. Optical density (OD) values were evaluated at 492 nm using a microplate reader (Labsystems Dragon Wellscan MK3, Finland).

In addition to the MTT assay, cell proliferation was measured using a cell counting kit-8 (Supporting Information, Figure S3)

*2.3.3. Cell-Image Analysis in Vitro.* At the end of 1, 3, 5, and 7 days of culturing time, the old culture medium was removed from the six-well plate, and an equal quantity of fresh $\alpha$-MEM was added. Fluorescein diacetate (FDA, Sigma) and propidium iodide (PI, Sigma) were simultaneously added to each well to final concentrations of 100 $\mu$g/mL and 60 $\mu$g/mL, respectively, on the basis of previously described uses of FDA and PI.[32]

For the cell-adhesion studies, after cells were seeded onto the PET-ALs and G-PET-ALs and cultured for 1 and 2 days in $\alpha$-MEM supplemented with 10% FBS, the cells were fixed in 4% paraformaldehyde for 30 min, washed three times with PBS, permeabilized in 0.1% Triton X-100 for 20 min, and washed three times with PBS. After being blocked with 1% bovine serum albumin (BSA) for 30 min at room temperature, the cells were incubated with 10 $\mu$g/mL primary antivinculin antibody (Cat. No. ab129002, abcam) for 12 h at 4 °C. After being washed three times with PBS, the cells were incubated with fluorescein isothiocyanate (FITC)-labeled goat antirabbit IgG antibody (Abcam, USA) for 2 h. Tetramethyl rhodamine isothiocyanate (TRITC)-labeled phalloidin (Cytoskeleton, USA) was used to stain the actin cytoskeletons of the cells, which were then washed three times with PBS after 40 min. Afterward, the cell nucleus were stained with 4′,6-diamidino-2-phenylindole (DAPI) for 5 min, and the cells were then washed three times with PBS. The scaffolds were mounted on coverslips and examined using a confocal laser scanning microscope (TCS SP5, Leica, Solms, Germany). Projected cell area was analyzed from the images of cytoskeleton organization (red), and integral optical density (IOD) values were analyzed from the images of immuno-staining of vinculin (green) by Image pro-Plus6.0 software.

*2.3.4. Histochemical Staining for Alkaline Phosphatase (ALP).* The histochemical detection of ALP was performed using a BCIP/NBT (5-bromo-4-chloro-3-indoly phosphate and nitro blue tetrazolium) ALP staining kit (Cat. No. C3206, Beyotime). When the MC3T3-E1 cells were 80−90% confluent on the fibrous scaffolds, they were inducted in osteoinductive medium, 10% v/v FBS and DMEM (Dulbecco's modification of Eagle's medium) with 4.5 g/L glucose, 10 mM sodium $\beta$-glycerophosphate, 50 $\mu$g/mL vitamin C, 1 × $10^{-8}$ mM dexamethasone, 100 U/mL penicillin, and 100 U/mL streptomycin, for 7 days and 14 days; then, the cells were washed three times with PBS, fixed in ice-cold acetone (4 °C) for 2 min, and then washed thrice with PBS (pH 7.4).

Afterward, Tris-buffered staining solution was added; the color development was terminated after 1 h by washing with PBS, and the staining was then examined under a microscope.

*2.3.5. ALP Activity Assay.* ALP activity was assayed using an ALP assay kit (Cat. No. P0321, Beyotime). The MC3T3-E1 cells were treated with osteoinductive medium for 7 days and 14 days. The cells were washed thrice with PBS and then harvested via trypsinization. The harvested cells were centrifuged at 375 × g for 5 min. Afterward, 200 $\mu$L of 0.1% Triton X-100 (Sigma) was added to lyse the cells, and the cells were sonicated twice on ice. Then, the fragmentized cells were centrifuged at $10^4$ × g for 20 min at 4 °C. The supernatants were analyzed for ALP activity. The absorbance was determined at 405 nm using a microplate reader (Labsystems Dragon Wellscan MK3, Finland). ALP activity was measured in units of nmol of p-nitrophenol released per min per $\mu$g of protein.

*2.3.6. Evaluation of the Formation of Mineralized Bone Nodules via Histochemical Analysis and Quantitation Assay.* Alizarin Red S staining was used as an indicator of bone-nodule formation. The MC3T3-E1 cells were treated with osteoinductive medium for 21 days and 28 days, and at the end of each period, the cells were rinsed in PBS and fixed in ice-cold ethanol for 5 min. The cells were then stained with 0.5% Alizarin Red S (pH 4.3, Sigma) for 30 min at RT and washed with PBS until there was no Alizarin Red S dye in the water, and the staining was examined via photography. To quantify the amount of Alizarin Red S bound to the mineralized nodules, cells were rinsed with PBS and extracted with 10% (w/v) cetylpyridinium chloride (Sigma) for 1 h at RT. The dye concentration in the extract was determined at OD 572 nm.

*2.3.7. Real-Time Polymerase Chain Reaction (RT-PCR) Analysis.* RT-PCR analysis is a method of monitoring the transcription levels of osteoblast differentiation markers such as runt-related transcription factor 2 (Runx2); osteocalcin (OCN); osteopontin (OPN); and collagen, type I, alpha 1 (COL1A1). In brief, the total messenger ribonucleic acid (mRNA) of the MC3T3-E1 cells was isolated after induction in osteoinductive medium for 7, 14, and 21 days using TRIzol (Takara); then, 2 $\mu$L of mRNA was transcribed to 20 $\mu$L of complementary DNA using PrimeScript RT Master Mix (Cat. No. RR036A, Takara). Then, 12.5 $\mu$L of SYBR Premix Ex *Taq*II 2X (Cat. No. RR820, Takara), 1 $\mu$L of PCR Forward Primer (Takara) and PCR Reverse Primer (Takara), 2 $\mu$L of cDNA, and 8.5 $\mu$L of sterilized distilled water were added. RT-PCR reactions were performed according to the following cycling program: initial denaturation at 95 °C for 15 min, followed by 40 cycles of 15 s of amplification consisting of denaturation at 95 °C, 45 s of annealing at 62 °C, and an extension step at 60 °C for 1 min. The primers used are listed in Table 1.

**2.4. Animal Experiments.** *2.4.1. Implantation Surgery Procedure.* The animal experiments were approved by the Institutional Animal Care and Use Committee at our institution. Thirty-two mature New Zealand rabbits (male, 12 weeks old, 3.0 ± 0.4 kg) were subjected to an operative extra-
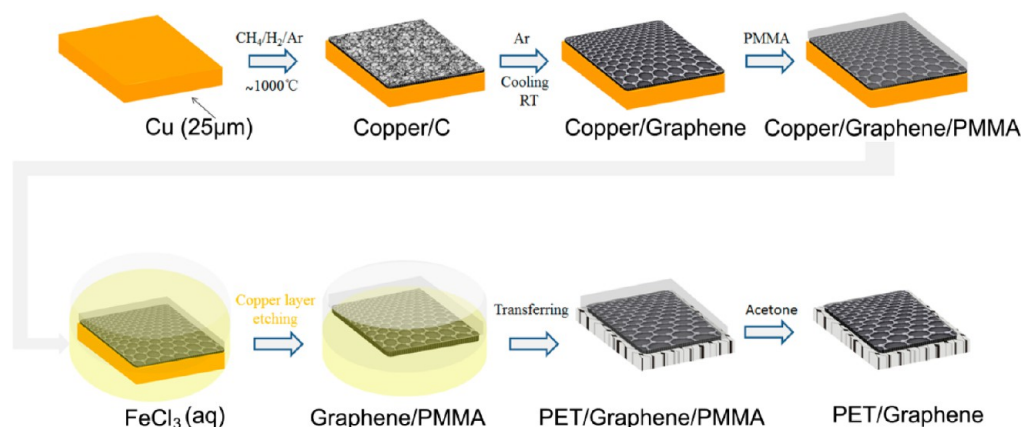
**Figure 1.** Illustration of the growth, etching, and transferring processes of the CVD-grown large-scale graphene films.
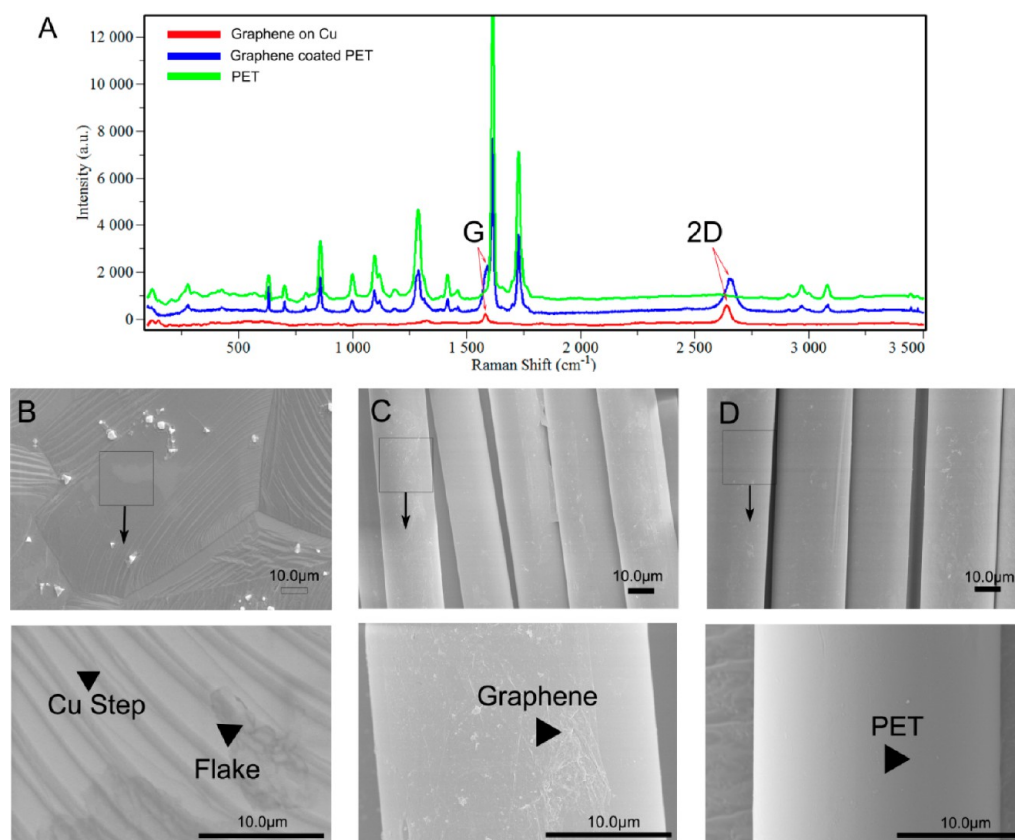


**Figure 2.** (A) Raman spectra (633 nm laser wavelength) obtained from a pure PET-AL scaffold, graphene on a copper foil, and G-PET-AL scaffold. G-band (1580 cm$^{-1}$) and 2D-band (2680 cm$^{-1}$) peaks are the major Raman features of graphene ($n = 4$). (B) SEM image of graphene on a copper foil with a growth time of 10 min ($n = 3$); inset shows high-resolution SEM image showed graphene flakes and Cu steps. (C) SEM image of pure G-PET-AL scaffold; inset shows high-resolution SEM image of pure G-PET-AL scaffold ($n = 3$). (D) SEM image of PET-AL scaffold; inset shows high-resolution SEM image of PET-AL scaffold ($n = 3$).

articular graft-to-bone healing procedure. The rabbits received no food or water for 12 h before the surgery. The rabbits were anaesthetized with xylazine hydrochloride injection (intramuscular injection, 1 mg/kg) and 3% pentobarbital (intramuscular injection, 30 mg/kg). After disinfection and incision, tunnels were drilled using a 4 mm-diameter aiguille through the condyle of the femur. All grafts had a length of 3.0 cm and a diameter of 4.0 mm. A G-PET-AL graft was implanted into one limb, and a PET-AL graft was implanted into the contralateral limb as the control. Then, the wound was closed in layers. Postoperatively, gentamicin (5 mg/kg) and penicillin (50 KU/

kg) were administered through continuous injection for 3 days. The rabbits were sacrificed at 4, 8, and 12 weeks after surgery for the examinations described below.

*2.4.2. Mechanical Tests.* Six specimens from each group were used for mechanical tests. Each specimen was divested of all soft tissue, and a No. 5 ETHIBOND suture was used to suture the graft, extending out of the lateral tunnel entrance. Afterward, the specimens were mounted onto a special jig without being frozen. The jig was adjusted to ensure that the tension on each graft was applied solely along its long axis. Once each specimen was tightly secured, an axial pullout test

**Table 2. Scaffold Characterization ($n = 6$, Mean $\pm$ SD)**

| scaffold | water contact angle (deg) | porosity (%) | ultimate failure load (kN) | stiffness (N/mm) |
|---|---|---|---|---|
| G-PET-AL[b] | $53.8 \pm 2.5^a$ | $58.2 \pm 0.5$ | $2.3915 \pm 0.1909$ | $50.5 \pm 3.73$ |
| PET-AL[b] | $83.1 \pm 5.9$ | $58.5 \pm 0.3$ | $2.3337 \pm 0.2133$ | $47.5 \pm 2.51$ |

[a]Significant difference was found compared with the control group ($p < 0.05$). [b]G-PET-AL indicates graphene-coated PET artificial ligament; PET-AL indicates PET artificial ligament.
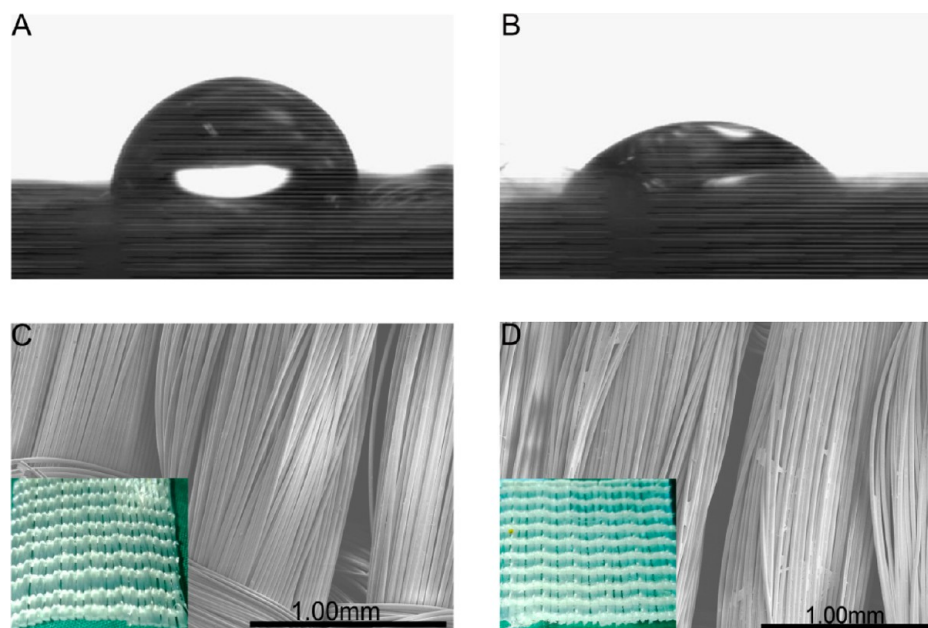


**Figure 3.** Water contact angle images of (A) pure PET-AL scaffold and (B) G-PET-AL scaffold ($n = 6$). SEM images of (C) pure PET-AL scaffold and (D) G-PET-AL scaffold ($n = 3$). Inset in panel C shows digital camera image of a pure PET-AL scaffold. Inset in panel D shows digital camera image of a G-PET-AL scaffold.

was performed using a Material Testing System, Model 858 (MTS Systems, Minneapolis, MN). The load-to-failure test was performed at an elongation rate of 2 mm/min.[33] The tensile load and elongation were recorded and used to determine the ultimate failure load (N) and the stiffness (N/mm). The stiffness was determined from the slope of the load deformation curve. After each graft was pulled out through the lateral tunnel entrance, the femur condyles and grafts were embedded in methyl methacrylate (MMA). Pathological sections were cut and stained with Van Gieson (VG).

*2.4.3. Micro-CT Examination.* The rabbits were randomly sacrificed at 4, 8, and 12 weeks after surgery, and the femur condyles were then carefully dissected and fixed in 80% ethanol for 2 weeks. The specimens were placed in a sample holder and scanned at an isotropic resolution of 18 $\mu$m using a Micron X-ray 3D Imaging System (Y. Cheetah, Germany). For each specimen, a $4 \times 10$ mm$^2$ cylindrical region of interest from the middle portion of the bone tunnel along its longitudinal axis was reconstructed and analyzed at a threshold of 2000 using VGStudio MAX (Volume Graphics, Germany) software. The bone volume/total volume (BV/TV, %), bone surface/bone volume (BS/BV, 1/mm), trabecular thickness (TbTh, mm), trabecular number (TbN, 1/mm), and trabecular spacing (TbSp, mm) were determined.

*2.4.4. Histological Observations.* The animals were labeled with tetracycline (intramuscular injection, 50 mg/kg, Sigma) and calcein (intramuscular injection, 8 mg/kg, Sigma) 14 and 4 days, respectively, before being sacrificed at each time point. Then, the animals were euthanized, and the femur condyles

were fixed in 80% ethanol for 2 weeks. At each time point, the specimens were dehydrated in a graded ethanol series (70–100%) within a span of 24 h; then, the specimens were embedded in MMA solution for 3 weeks. After polymerization of the MMA at 50 °C for 24 h, pathological sections were cut using a band saw and observed using a fluorescence microscope. The mineral apposition rate (MAR) of new bone formation was measured by monitoring the length between the two labels over time ($\mu$m/d). After the observation of fluorochrome double labeling, the bone sections were stained with VG stain and observed under a light microscope; the newly formed bone was stained red. The graft-to-bone healing was evaluated based on two parameters: the newly formed bone in the bone tunnel and the bonding of the graft to the adjacent tissue. Bone formation was qualitatively analyzed by the VG staining of pathological sections using Image Pro Plus 17.0.

**2.5. Statistical Analyses.** All data were analyzed using SPSS 10.0 and Graphpad Prism 5 statistical software. Each set of results presented is representative of at least three separate experiments. The results are expressed as the mean $\pm$ SD, and significant differences were evaluated using the paired Student's $t$-test. Significance was assigned at $p < 0.05$.

## 3. RESULTS

**3.1. Preparation of PET-ALs and G-PET-ALs.** As shown in Figure 2, panel B, the large-scale CVD-grown graphene on copper foils were characterized via SEM. An analysis of the SEM image of the entire sample indicated that the area exhibiting the lightest color was greater than 95% of the whole.
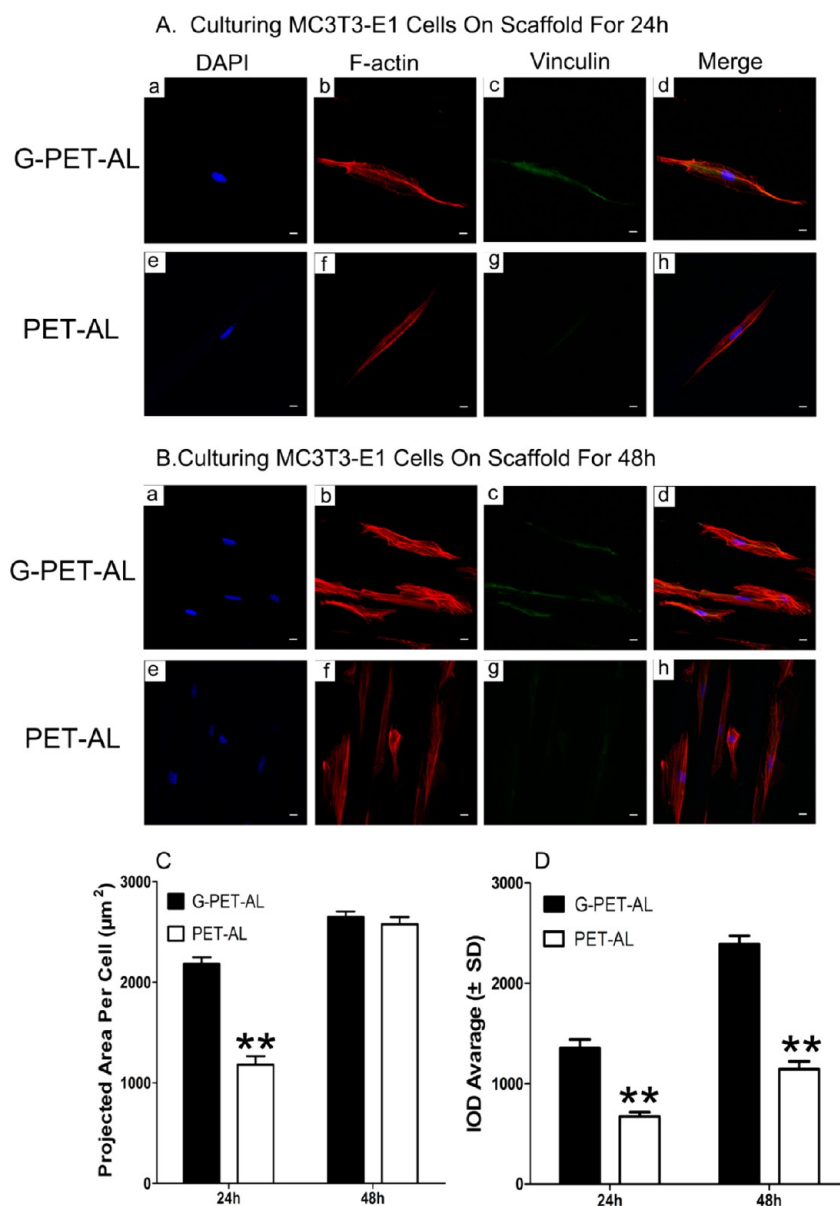
**Figure 4.** (A) Confocal laser scanning microscope images of MC3T3-E1 cells incubated 24 h on (a−d) G-PET-AL scaffold and (e−h) PET-AL scaffold ($n = 3$). (B) The fluorescent images of MC3T3-E1 cells incubated 48 h on (a−d) G-PET-AL scaffold and (e−h) pure PET-AL scaffold ($n = 3$). Panels a and e show DAPI immunostaining of DNA (blue). Panels b and f show staining of cytoskeleton organization (red). Panels c and g show immunostaining of vinculin (green). (C) Projected cell area, and (D) IOD were analyzed from the fluorescent images. Results are presented as mean ± standard error of the mean; * indicates $p < 0.05$, and ** indicates a significant difference $p < 0.001$. Scale bars, 100 $\mu$m.

High-resolution SEM image of graphene on a copper foil (Figure 2B) showed that the lightest color was covered with graphene flakes. Figure 1 presented a schematic diagram of the growth, etching, and transference processes used for the graphene films. After the graphene coatings were applied to the surfaces of the PET-AL scaffolds, SEM was used to characterize the surfaces, as shown in Figure 2, panel C. High-resolution SEM image of graphene on PET-AL (Figure 2C) showed that there were graphene wrinkles on the surface of G-PET-AL. The results of Raman spectroscopy are presented in Figure 2, panel A. As is well-known, the G-band ($1560-1620$ cm$^{-1}$) and the 2D band ($2660-2700$ cm$^{-1}$) are the major Raman features of graphene. These features were used for graphene identification in this study.

**3.2. Scaffold Characterization.** The results of the characterization of the PET-ALs and G-PET-ALs are summarized in Table 2. To investigate the change in wettability of the materials, the water contact angle was measured before and after the application of the graphene coating (Figure 3A,B). We reasoned that graphene coating should effectively modify the wettability of the PET-AL scaffold ($p < 0.05$). In the field of bone-tissue engineering, the porosity of a scaffold is a key property in determining the ability to obtain a physiological cell distribution.[34] The gross morphology and SEM observations of the PET-AL grafts revealed high porosity (Figure 3C). After the application of the graphene coating, the coating seemed to be stably conjoined to the surfaces of the fibers (Figure 3D). The porosities of the PET-ALs and G-PET-ALs were measured using the liquid-displacement method, and the results are reported in Table 2. The results indicated that there was no significant difference between the PET-ALs and G-PET-ALs ($p = 0.353$). The ultimate failure loads (kN) and stiffnesses (N/

mm) of the pure PET-AL and G-PET-AL grafts were measured. The results are reported in Table 2. The graphene-coated scaffolds exhibited no significant difference in ultimate failure load ($p = 0.2974$) or stiffness ($p = 0.1174$) compared with the pure PET-AL grafts.

**3.3. Cell Attachment and Proliferation.** To investigate the biocompatibility of the PET-ALs and G-PET-ALs investigated in our study, the morphology of MC3T3-E1 cells was observed after 24 and 48 h of culturing. Figure 4, panels A and B present the immunostaining results for DNA (blue), F-actin (red), and vinculin (green) and the merged results for MC3T3 cells on PET-AL and G-PET-AL scaffolds. After 24 h of culturing, the cells were well distributed on the graphene-coated scaffolds. As shown in Figure 4, panel C, the projected cell area was $2184.6 \pm 169.4 \ \mu m^2$. A narrow and elongated morphology was observed on the pure PET-AL scaffolds, and the cell area decreased to $1179.7 \pm 226.5 \ \mu m^2$. After 48 h of culturing, there was no significant difference between the cell areas on the pure and graphene-coated PET-AL scaffolds ($p = 0.06916$). The IOD results (Figure 4D) for the vinculin immunostaining revealed that regardless of the cell-culturing time, there was a significant difference in focal adhesion between the G-PET-AL and PET-AL scaffolds ($p < 0.05$). SEM images (Figure 5A) revealed that the MC3T3-E1 cells that were
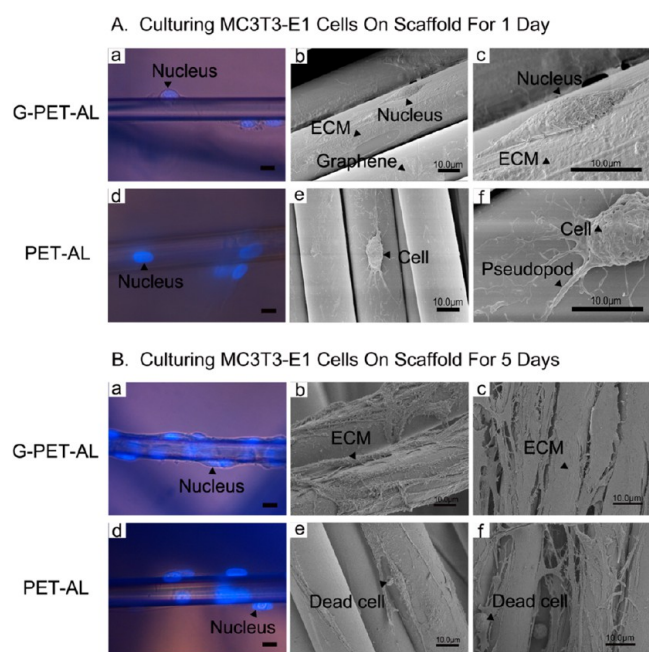


**Figure 5.** Fluorescent images of DAPI immunostaining of cell nucleus of MC3T3-E1 cells (blue) incubated (A: a, d) 1 day and (B: a, d) 5 days on each scaffold ($n = 3$). SEM images of MC3T3-E1 cells incubated (A: b, c) 1 day and (A: e, f) 5 days on a G-PET-AL scaffold ($n = 3$). SEM images of MC3T3-E1 cells incubated (B: b, c) 1 day and (B: e, f) 5 days on a pure PET-AL scaffold ($n = 3$). Scale bars, 100 $\mu m$.

attached to the G-PET-AL scaffolds presented more cellular pseudopods than did those on the PET-AL scaffolds after 1 day of culturing. After 5 days of culturing (Figure 5B), a greater amount of extracellular matrix (ECM) was observed covering the fibers of the G-PET-AL scaffolds than was observed covering those of the PET-ALs.

The MC3T3-E1 cells that were cultured on the PET-AL and G-PET-AL scaffolds were evaluated after 1, 3, 5, and 7 days of incubation. The results were assessed via an MTT assay (Figure

6A). The OD value was significantly different between the PET-AL and G-PET-AL groups at all time points ($p < 0.05$). PI and FDA were used to identify live and dead cells. As shown in Figure 6, panel C, the numbers of both live and dead cells increased over time in all three groups. The number of live cells on the G-PET-AL scaffolds was significantly greater than that on the PET-AL scaffolds at each time point ($p < 0.05$).

**3.4. Cell Differentiation.** Because ALP is an early marker for the osteogenous differentiation of cells, after 7 and 14 days of culturing, histochemical detection was performed to determine ALP activity (Figure 7A). The results suggested that the ALP expression in the G-PET-AL group was higher than that in the PET-AL group. Moreover, the ALP activity in the G-PET-AL group was significantly higher at the indicated time points ($p < 0.05$). After 21 and 28 days of induction, Alizarin Red S staining and quantitation were performed. In the images of Alizarin Red S staining (Figure 7D), we found that obvious calcium-salt sedimentation occurred in the G-PET-AL group. Quantification of the Alizarin red S stain bound to the calcium nodules (Figure 7C) showed that there was significantly higher calcification in G-PET-ALs compared with that in PET-ALs ($p < 0.05$).

The transcription levels of osteoblast-specific genes, including Runx2, OCN, OPN, and COL1A1, were evaluated via RT-PCR (Figure 8). The transcription levels of the Runx2, OCN, OPN, and COL1A1 genes were $0.23 \pm 0.07$-fold, $0.27 \pm 0.06$-fold, $0.13 \pm 0.03$-fold, and $1.01 \pm 0.07$-fold on the G-PET-AL scaffolds, respectively, and $0.14 \pm 0.07$-fold, $0.15 \pm 0.03$-fold, $0.06 \pm 0.02$-fold, and $0.15 \pm 0.04$-fold on the PET-AL scaffolds, respectively, at 7 days. The transcription levels of these osteoblast-specific genes in the cells on the G-PET-AL scaffolds were significantly upregulated with respect to the cells on the PET-AL scaffolds at 7 days ($p < 0.05$). After 14 and 21 days, the same transcription levels were observed ($p < 0.05$).

**3.5. Mechanical Tests.** As shown in Figure 9, panels C and D, at 4 weeks after surgery, the PET-AL group presented an ultimate failure load of $26.17 \pm 0.65$ N and a stiffness of $7.22 \pm 0.53$ N/mm. The G-PET-AL group exhibited the higher ultimate failure load and stiffness, $46.18 \pm 3.33$ N and $14.6 \pm 1.93$ N/mm, respectively, compared with the PET-AL group ($p < 0.05$). At 8 weeks, the ultimate failure load and stiffness in the G-PET-AL group were $63.88 \pm 6.09$ N and $26.65 \pm 3.21$ N/mm, respectively, and they were significantly higher than those of the PET-ALs group ($p < 0.05$). At 12 weeks after surgery, the ultimate failure load and stiffness in the G-PET-AL group were 70.3% and 74.4% of those of the native ACL, respectively, and in the PET-AL group, they were 45.7% and 44.6% of those of the native ACL, respectively ($p < 0.05$).

**3.6. Micro-CT Examinations.** Identically sized areas of interest (AOIs) around the scaffolds were reconstructed and imaged (Figure 10). We observed that there were more bone trabeculae around the scaffolds in the G-PET-AL group than in the PET-AL group. The microstructural parameters are presented in Table 3. At the 4-week time point, the BV/TV, TbTh, and TbN of G-PET-AL were significantly higher than those of the PET-AL group ($p < 0.05$) as well as there were significant decreases in BS/BV and TbSp ($p < 0.05$). At 8 weeks and 12 weeks, in the G-PET-AL group, the BV/TV, TbTh, and TbN gradually increased, and BS/BV and TbSp gradually decreased, and there was a significant difference between the G-PET-AL scaffolds and the PET-AL scaffolds at each time point ($p < 0.05$).
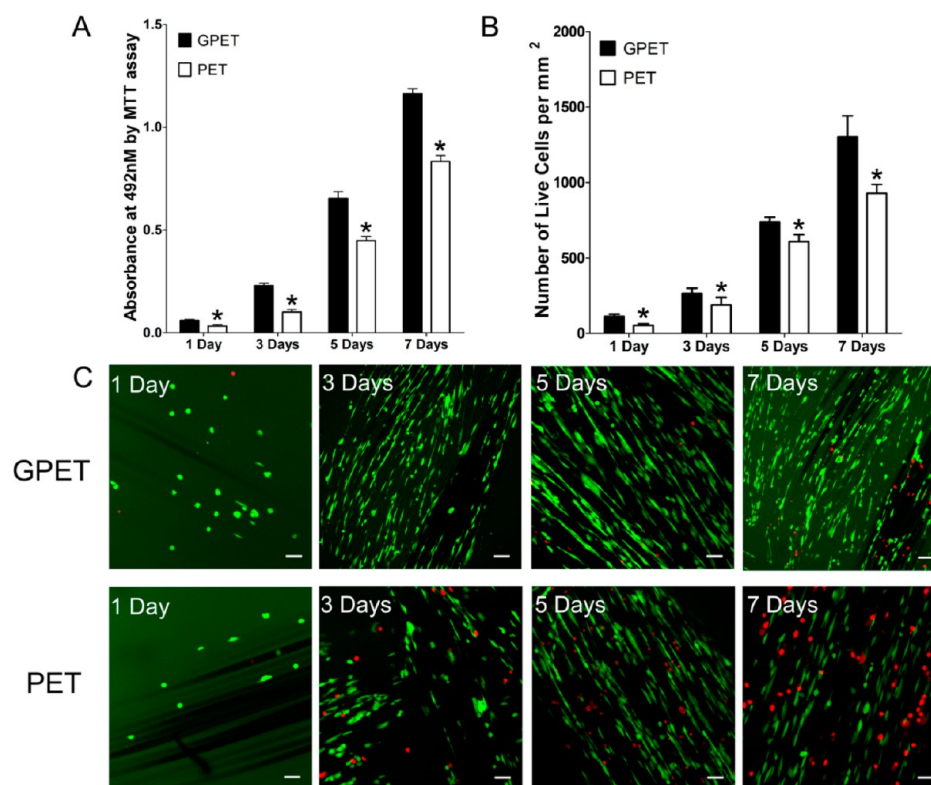
**Figure 6.** (A) The OD value of G-PET-AL group and PET-AL group at 1, 3, 5, and 7 days ($n = 7$). (B) The number of live cells per mm$^2$ ($n = 7$) was analyzed from the fluorescent images of panel C. The fluorescent images of live and dead cells after MC3T3-E1 cells cultured (C: a, e) 1 day, (C: b, f) 3 days, (C: c, g) 5 days, and (C: d, h) 7 days on each scaffold ($n = 3$). Results are presented as mean ± standard error of the mean; ∗ indicates $p < 0.05$, ∗∗ indicates a significant difference $p < 0.001$. Scale bars, 100 μm.

**3.7. Histological Observations.** At the 8-week time point, histological observations of strong tetracycline labeling (yellow bands) and calcein labeling (green bands) around the scaffolds using a fluorescence microscope revealed that the intervals between the centers of the yellow and green bands were 40.8 ± 3.5 μm on the G-PET-AL scaffolds and 26.5 ± 2.8 μm on the PET-AL scaffolds. The mineral apposition rate (Figure 11e) was significantly different between the G-PET-AL and PET-AL groups ($p < 0.05$). VG staining was used to assess graft-to-bone healing in the G-PET-AL and PET-AL groups. As shown in Figure 12, panel A, after 4 weeks, we observed that new bone had formed in the bone tunnel in the G-PET-AL group, but no new bone had formed in the PET-AL group. The new BV/PV of G-PET-ALs group (9.24 ± 1.32%) was significantly higher than that of the PET-ALs (4.27 ± 0.35%, $p < 0.05$), and the newly formed bone was bonded tightly to the G-PET-AL grafts. By contrast, between the newly formed bone and the PET-AL grafts, there was a great deal of soft tissue that exhibited yellow staining. After 8 weeks, more new bone had formed for both the G-PET-AL and PET-AL grafts. The observations indicated that the new bone spread to the inner region through the interspaces between the bundles in the G-PET-AL grafts. However, in the PET-AL grafts, very little newly formed bone was observed in the inner region. The BV/TV in G-PET-ALs (18.74 ± 2.13%) was markedly higher than that in PET-ALs (9.73 ± 1.24%, $p < 0.05$), and the osseointegration between the PET-AL graft and the new formed bone was weak, with additional soft tissue between the graft and the newly formed bone. At 12 weeks after surgery, most of the interspaces in the G-PET-AL grafts were filled with newly formed bone. The BV/PV of G-PET-ALs group (29.82 ± 4.26%) was significantly
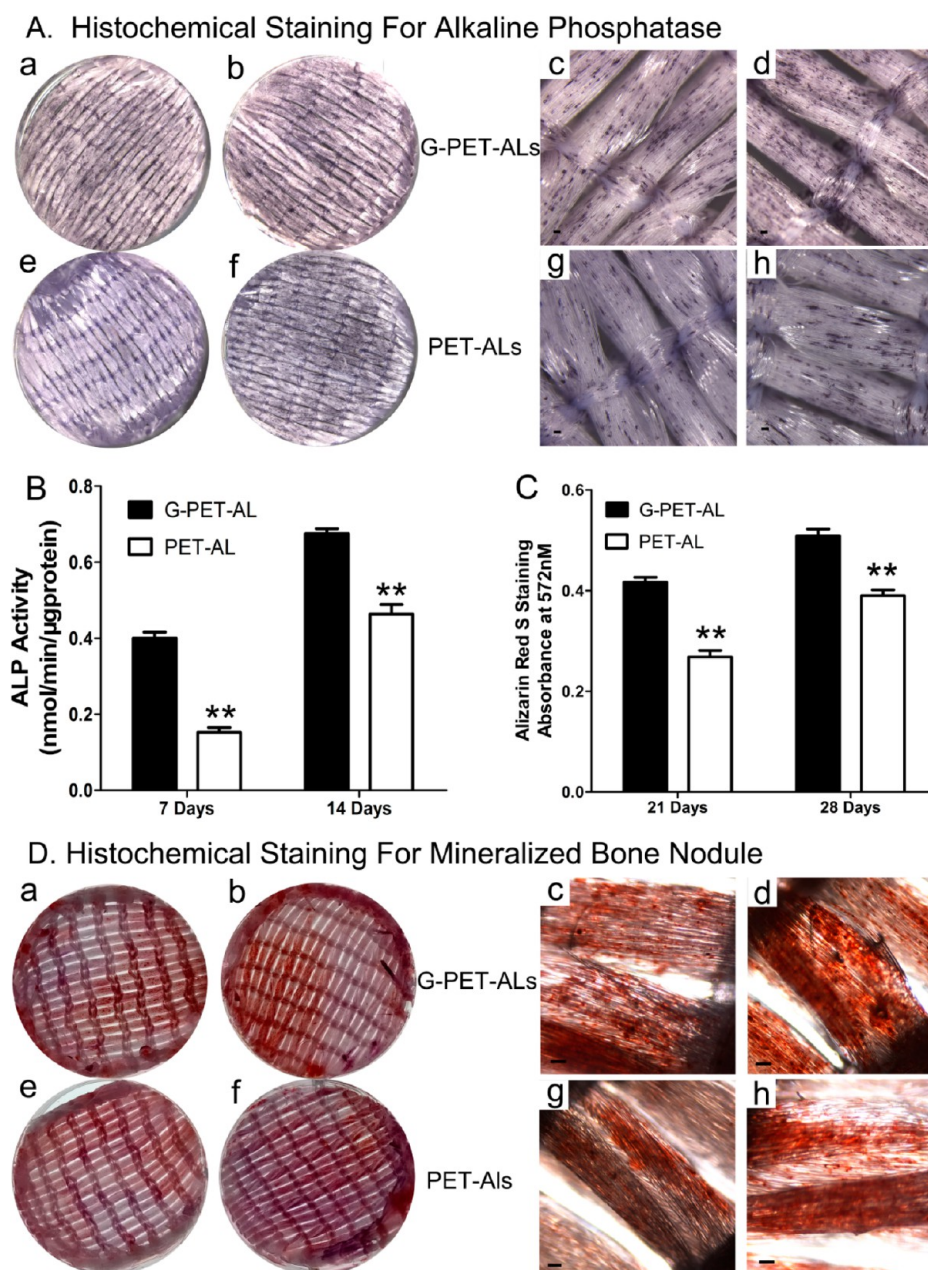
higher than that of the PET-ALs (17.98 ± 2.17%, $p < 0.05$). Although the amount of newly formed bone that was present had significantly increased in the PET-AL grafts compared with that observed at 8 weeks, the new bone formation in the bone tunnels and the bonding of the grafts to adjacent tissue were inferior to those observed for the G-PET-AL grafts.

## 4. DISCUSSION

Artificial ligament made from PET is commonly used for primary ACL reconstructive surgery. However, the low bioactivity of PET artificial ligaments is a major limitation for their clinical application. The objective of this study was to optimize the PET artificial ligaments and to improve their bioactivity. To this end, we coated graphene onto PET-ALs. Our results showed that the graphene layer was coated stably onto the surfaces of the PET artificial ligaments and enhanced the proliferation and osteogenic differentiation of MC3T3-E1 cells in vitro and improved the graft-to-bone healing in vivo.

As previously reported,[38] the major Raman features of graphene are the so-called G-band (1560−1620 cm$^{-1}$) and the 2D band (2660−2700 cm$^{-1}$). When the PET-AL sheets were coated with graphene, peaks appeared at 1560−1620 cm$^{-1}$ and 2660−2700 cm$^{-1}$; they were not present in the control group. In Figure 2, panel A, the red arrows marked the G-band (1580 cm$^{-1}$) and 2D (2680 cm$^{-1}$) band, respectively, and the red and blue lines are the Raman spectra of graphene-coated copper and graphene-coated PET scaffold, respectively. These changes suggest that we successfully coated the PET-AL with graphene. Ultrasonication test indicated that graphene layer was coated stably onto the surfaces of the PET-ALs (Supporting Information, Figure S1).

## A. Histochemical Staining For Alkaline Phosphatase



## D. Histochemical Staining For Mineralized Bone Nodule



**Figure 7.** Stereomicroscope images of histochemical staining for ALP after treated with osteoinductive medium for (A: a, c) 7 days and (A: b, d) 14 days on G-PET-AL scaffolds ($n = 3$). Histochemical staining for ALP at (A: e, g) 7 days and (A: f, h) 14 days on PET-AL scaffolds ($n = 3$). (B) The ALP activity of each scaffold at 7 and 14 days ($n = 3$). (C) Intensity of Alizarin red S stain bound to calcium nodules. The OD values for Alizarin red S staining (572 nm) at 21 and 28 days ($n = 3$). (D) Digital camera images of Alizarin Red S staining of mineralized bone at (D: a, c) 21 days and (D: b, d) 28 days on G-PET-AL scaffolds ($n = 3$). Alizarin Red S staining at (D: e, g) 21 days and (D: f, h) 28 days on PET-AL scaffolds ($n = 3$). * indicates $p < 0.05$, ** indicates a significant difference $p < 0.001$. Scale bars, 100 $\mu$m.

An ideal prosthesis should be accepted by the body and mimic the geometric structures and biological functions of native tissues, particularly for ligament-tissue engineering. Studies have demonstrated that graphene is capable of enhancing the adhesion, survival, proliferation, and differentiation of cells.[27,28] In our in vitro study, in both the G-PET-AL and PET-AL groups, the MTT OD increased with culturing time, indicating that PET-AL and G-PET-AL both promote the proliferation of MC3T3 cells. Moreover, it was observed that the graphene-coated group exhibited a higher OD at each time point ($p < 0.05$). PI and FDA staining (Figure 6C) indicated that there were more living cells (green) and fewer dead cells

(red) in the G-PET-AL group than in the pure PET-AL group. Cytoskeleton and vinculin staining revealed that after 24 h of culturing, the projected cell area of the PET-AL scaffolds was only 53.9% of that of the G-PET-AL scaffolds, and although the projected cell area was not significantly different after 48 h of culturing, more vinculin was observed in the G-PET-AL group at each time point. All evidence indicated that graphene modification enhanced the adhesion, survival, and proliferation of the MC3T3 cells. The biocompatibility of the PET-ALs has been significantly improved by graphene coating.

The differentiation of the MC3T3 cells was evaluated by monitoring the level of ALP activity as well as through the
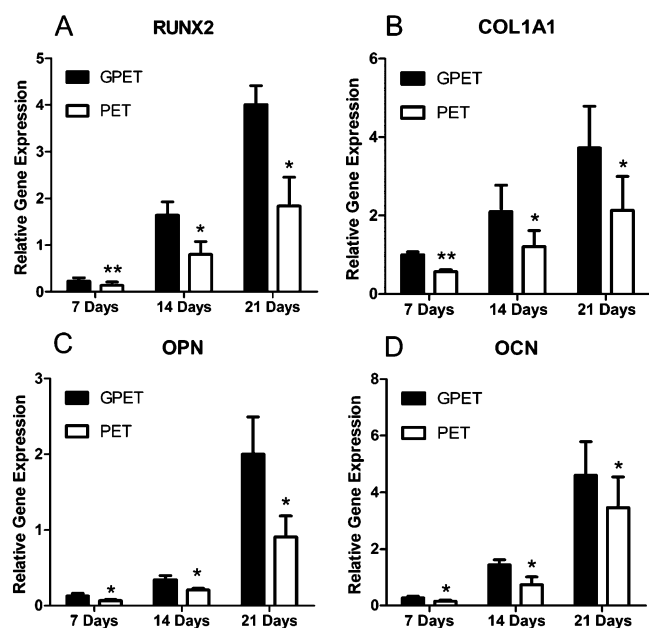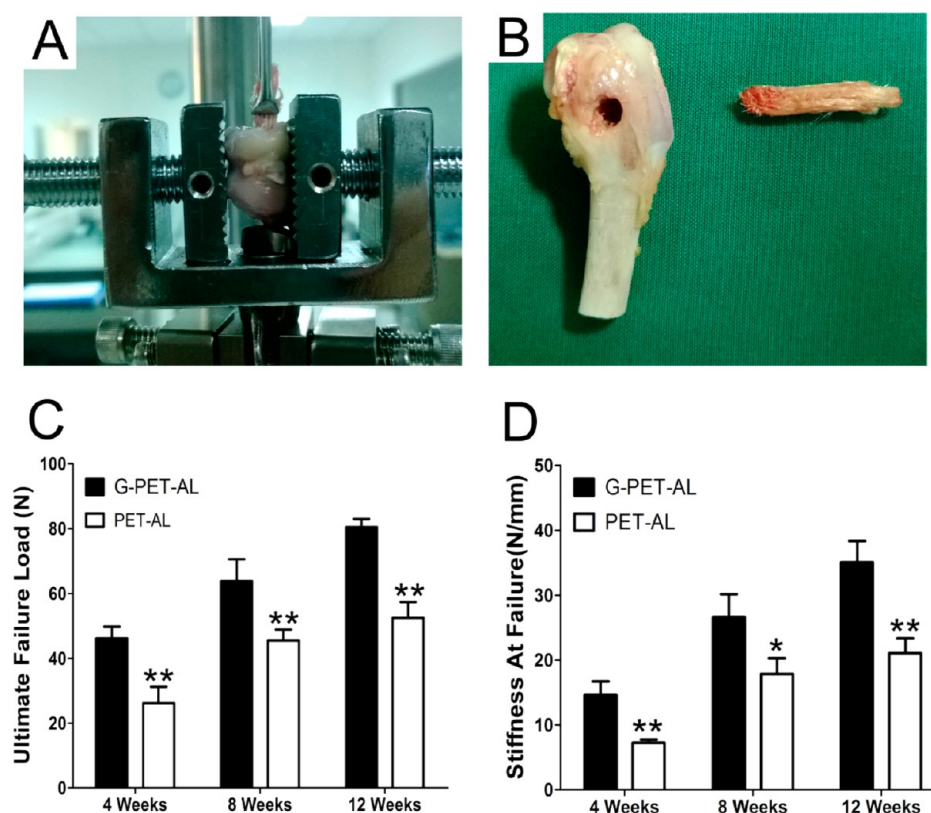
**Figure 8.** RT-PCR analysis of osteoblast-specific genes. Results are presented as mean ± standard error of the mean ($n = 3$); ∗ indicates $p < 0.05$, ∗∗ indicates a significant difference $p < 0.001$.

quantification of bone-nodule formation and the transcription levels of specific genes including collagen I, Runx2, OCN, and OPN. ALP is the earliest indicator of the differentiation of MC3T3 cells;[39] the results of histochemical detection regarding

ALP activity suggested that the ALP expression in the G-PET-AL group was higher than that in the PET-AL group. OCN and OPN are expressed at a later stage of the differentiation of MC3T3 cells.[39] Runx2 can directly stimulate the transcription of the encoding of OCN, COL1A1, and OPN.[40] As shown in Figure 8, the transcription levels of all genes in the cells on the G-PET-AL scaffolds were significantly upregulated with respect to those in the cells on the PET-AL scaffolds at 7, 14, and 21 days ($p < 0.05$). The results demonstrated that the presence of graphene had a positive influence on the differentiation of the MC3T3 cells. Thus, the in vitro study showed that graphene coating can improve the adhesion, proliferation, and differentiation of MC3T3 cells. We supposed that the outstanding surface activity of graphene could promote the PET-ALs' adsorption of the growth factor of the seeding cells, thus increasing the proliferation and differentiation of the cells. However, the pathway, through which graphene influence the proliferation and differentiation of cells, is still not clear. In the following experiment, we will focus on researching its mechanism of promoting the proliferation and differentiation of the cells.

At the enthesis of a native ACL, the fibrocartilage comprises four tissues: ligament, unmineralized fibrocartilage, mineralized fibrocartilage, and bone.[35] For ease of surgical ACL reconstruction, artificial ligaments must promote fibrocartilage development and maturation in and around the prosthesis for the purposes of integration and the formation of a strong interface with the bone.[36] In our in vivo study, rabbits were used to establish the extra-articular graft-to-bone healing



**Figure 9.** (A, B) Digital camera image of the condyle of femur and implant before and after the implant was pulled out of the lateral tunnel entrance of femur. (C) The ultimate failure load of each implant at 4, 8, and 12 week time points ($n = 5$). (D) The stiffness of each implant at 4, 8, and 12 week time points ($n = 5$). Results are presented as mean ± standard error of the mean; ∗ indicates $p < 0.05$, ∗∗ indicates a significant difference $p < 0.001$.
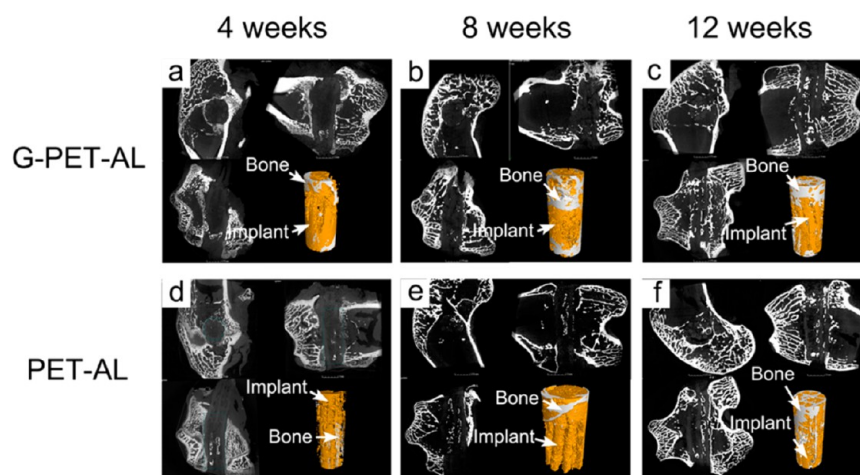
**Figure 10.** 3D reconstruction of G-PET-ALs and PET-ALs implants after implanted (a, d) 4 weeks, (b, e) 8 weeks, and (c, f) 12 weeks. The white color component was newly formed bone in these scaffolds, $n = 5$.

**Table 3. Results for Microstructural Parameters ($n = 5$, Mean $\pm$SD)[c]**

|  | 4 weeks | | 8 weeks | | 12 weeks | |
|---|---|---|---|---|---|---|
|  | G-PET-AL | PET-AL | G-PET-AL | PET-AL | G-PET-AL | PET-AL |
| BV/TV (%) | 8.84 ± 0.34[b] | 3.43 ± 0.25 | 19.16 ± 1.36[b] | 9.93 ± 0.75 | 26.43 ± 3.76[a] | 18.61 ± 1.47 |
| BS/BV (1/mm) | 8.3805 ± 1.12 | 16.1457 ± 5.3 | 13.23 ± 0.67[a] | 17.204 ± 2.11 | 12.6534 ± 1.78[a] | 14.3721 ± 1.21 |
| TbTh (mm) | 0.2386 ± 0.07[b] | 0.0765 ± 0.002 | 0.1512 ± 0.06[a] | 0.1163 ± 0.08 | 0.15806 ± 0.096[a] | 0.1392 ± 0.004 |
| TbN (1/mm) | 0.8705 ± 0.75[b] | 0.4489 ± 0.103 | 1.2676 ± 0.14[b] | 0.8545 ± 0.26 | 1.6721 ± 0.32[a] | 1.3371 ± 0.05 |
| TbSp (mm) | 1.8602 ± 1.37[a] | 2.1512 ± 0.303 | 0.6378 ± 0.24[a] | 1.05408 ± 0.37 | 0.4310 ± 0.054[b] | 0.6087 ± 0.004 |

[a]Significant difference was found compared with the control group ($p < 0.05$). [b]Significant difference was found compared with the control group ($p < 0.001$). [c]G-PET-AL indicates graphene-coated PET artificial ligament; PET-AL indicates PET artificial ligament. BV/TV indicates the bone volume/total volume, BS/BV indicates the bone surface/bone volume, TbTh indicates the trabecular thickness, TbN indicates the trabecular number, TbSp indicates trabecular spacing.

model[41] and evaluate the ability of the G-PET-AL scaffolds to improve graft-to-bone healing. As previously reported,[37] if the biocompatibility of ACL prosthesis was poor, an interposed layer of fibrous scar tissue, which was caused by the infiltration of inflammatory cells, would take the place of the fibrocartilage transitional zone after ACL surgical implantation. Preliminary long-term studies have demonstrated success rates of ACL construction ranging between 30 and 60%.[37] One of the major reasons for ACL reconstruction failure is that an interposed layer of fibrous scar tissue with poor mechanical properties takes the place of the fibrocartilage transitional zone after surgical implantation and makes it difficult for osteointegration at the interface between the artificial ligaments.[37] Thus, it is important to develop interventions that can promote fibrocartilage development and maturation in and around the prosthesis to enhance graft-to-bone healing. In this study, histology staining at 4 weeks (Figure 12A) indicated that the bone had bonded tightly to the G-PET-AL grafts; by contrast, there was a great deal of blue-stained fibroblast (F) at the interfaces between the scant newly formed bone and the PET-AL grafts. Histological observations of strong tetracycline labeling (yellow bands) and calcein labeling (green bands) around the scaffolds, which were acquired using a fluorescence microscope, demonstrated that the mineral apposition rate (Figure 11e) in the G-PET-AL group was significantly higher than that in the PET-AL group ($p < 0.05$). The results demonstrated that the presence of graphene had a positive influence on the regeneration and osteointegration of the bone tissue.

Micro-CT scans (Table 3) detected that the G-PET-AL group exhibited a 157.7% increases compared with PET-ALs in the BV/TV after 4 weeks. Therefore, it was presumed that the graphene promoted various growth factors in the bone marrow, thereby limiting scar formation and enhancing the adhesion and proliferation of bone in the tunnels. These findings appeared to correlate with an improvement in mechanical properties, which is a key consideration in ligament-tissue engineering. The ultimate failure load and stiffness predominantly corresponded to the newly formed bone. The ultimate failure load and stiffness differed significantly between the G-PET-AL group and the control group at 4, 8, and 12 weeks after surgery (Figure 9C,D). The results of Micro-CT scans (Table 3) and mechanical tests detected that compared with the BV/TV at 8 weeks, the rate of increase in BV/TV of the G-PET-AL group (37.94%) was lower than that of the PET-ALs (87.4%) at 12 weeks after surgery. Inconsistently, compared with the ultimate failure load at 8 weeks, the rate of increase in ultimate failure load of the G-PET-AL group (26.61%) was higher than that of the PET-ALs (15.48%) at 12 weeks after surgery. This discrepancy may be attributable to the presence of an interposed layer of fibrous scar tissue between the newly formed bone and the PET-AL grafts. At 12 weeks after surgery, the ultimate failure load and stiffness in the G-PET-AL group were 70.3% and 74.4% of those of native ACL, respectively. In this study, we hypothesized that the scaffold should be able to withstand the forces exerted at the knee during daily activities rather than the failure forces associated with trauma. Indeed, the 70.3% ultimate failure load and 74.4% stiffness compared
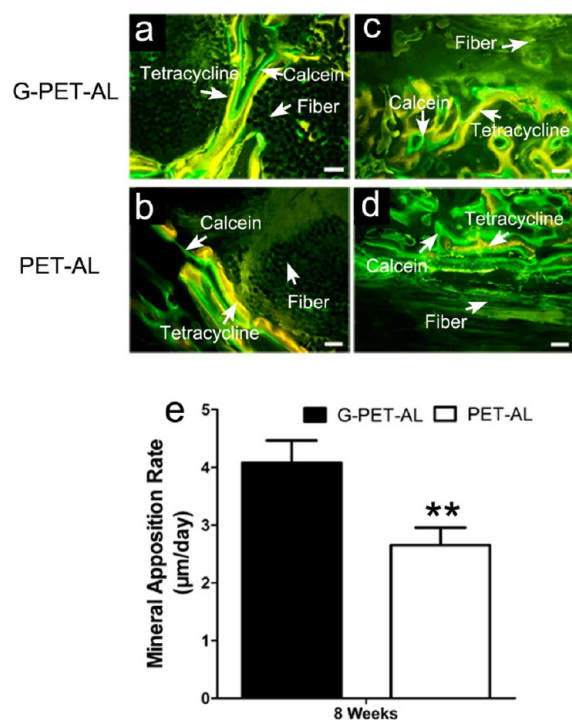
**Figure 11.** (a, b) Fluorochrome double-labeling of each scaffold sectioned to the horizontal axis at 8 weeks. (c, d) Fluorochrome double-labeling of each scaffold sectioned to the longitudinal axis at 8 weeks. (e) MAR of new bone formation of each scaffold at 8 weeks. Results are presented as mean ± standard error of the mean ($n = 12$); ∗ indicates $p < 0.05$, ∗∗ indicates a significant difference $p < 0.001$. Scale bars, 100 $\mu$m.

with native ACL that were observed for the G-PET-AL grafts are sufficient to withstand the forces associated with daily activities. The results demonstrated that the presence of graphene was important to promote fibrocartilage development and maturation in and around the prosthesis to enhance graft-to-bone healing.

The limitations of this study lie in the fact that the in vivo study used the rabbit extra-articular graft-to-bone healing model.[41] In contrast to the tibio-femoral (TF) joint model of ACL reconstruction,[42] the extra-articular graft-to-bone healing model can be used to investigate only the femoral portion of an artificial ligament. However, as in our previous study, we merely wished to investigate whether the properties of graphene could enhance graft-to-bone healing. To investigate the intra-articular portion of a graphene-coated artificial ligament in the synovial environment of the knee joint, a future study will focus on optimizing the model of ACL reconstruction, and more data will be needed.

## 5. CONCLUSIONS

In this study, PET-based artificial ligaments were fabricated using an independent knitting method. The technique of graphene coating resulted in the robust proliferation and differentiation into osteogenic lineages of MC3T3 cells on the fibrous PET scaffolds. After the implantation of a graphene-coated graft into the bone tunnel, the graft-to-bone healing was accelerated. Graphene coating may promote early recovery from ACL reconstruction. The objective of future studies must be to investigate the intra-articular portions of graphene-coated artificial ligaments. The findings of this study imply that
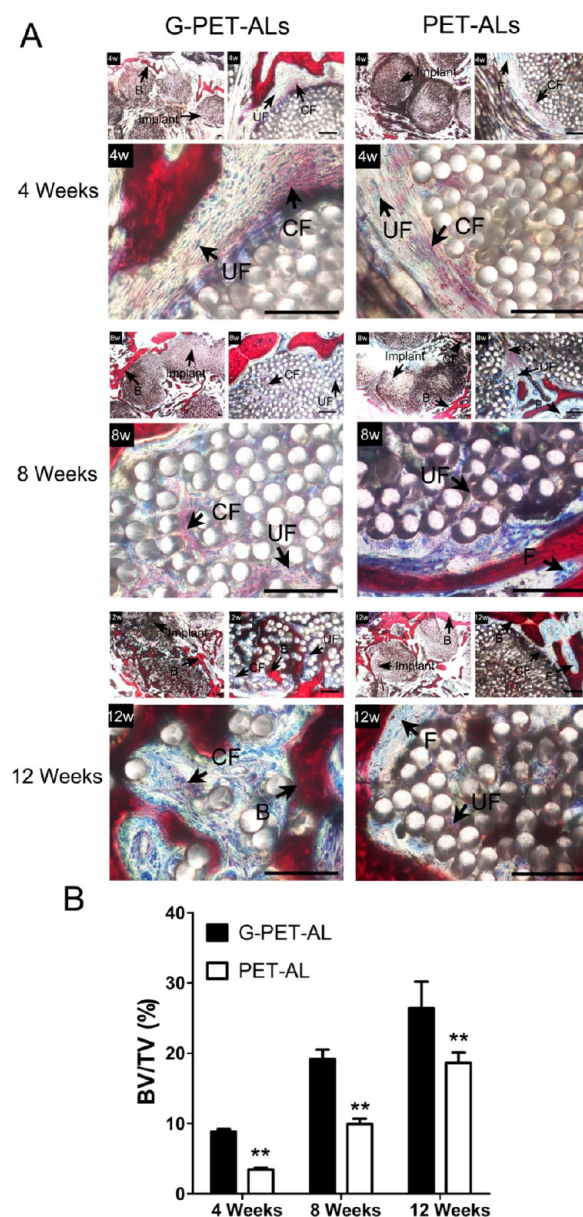


**Figure 12.** Light microscope images of VG staining of pathological sections of G-PET-ALs and PET-ALs groups at (A, B) 4 weeks, (C, D) 8 weeks, and (E, F) 12 weeks, respectively. The tissue stained in red color was the newly formed bone with visible cell nucleus. The tissue stained in dark blue color was fibroblast. (G) Histomorphometric measurement of new bone formation within the implants. Newly formed bone (B), uncalcified fibrocartilage (UF), calcified fibrocartilage (CF), fibroblast (F). ∗ indicates $p < 0.05$, ∗∗ indicates a significant difference $p < 0.001$. Scale bars, 100 $\mu$m.

graphene exhibits considerable potential for enhancing the surface bioactivation of materials.

## ■ ASSOCIATED CONTENT

**ⓢ Supporting Information**

SEM images of graphene sheets on the PET-ALs before and after ultrasonication treatment for 1 h. Raman spectroscopy analysis performed at a wavelength of 633 nm. Measurement of MC3T3-E1 cells proliferation by CCK-8 assay after 1, 3, 5, and 7 days of incubation. Microscope images when the cell become 80% confluent. The Supporting Information is available free of

charge on the ACS Publications website at DOI: 10.1021/acsami.5b02893.

## ■ AUTHOR INFORMATION

### Corresponding Authors
*Phone: 86-29-84775289. Fax: 86-29-84775289. E-mail: bilong@fmmu.edu.cn.
*Phone: 86-29-84773203. Fax:86-29-84773203. E-mail: drhanys@yeah.net.

### Author Contributions
§These authors contributed equally to this study.

### Notes
The authors declare no competing financial interest.

## ■ REFERENCES

(1) Widuchowski, W.; Widuchowski, J.; Koczy, B.; Szyluk, K. Untreated Asymptomatic Deep Cartilage Lesions Associated with Anterior Cruciate Ligament Injury: Results at 10- and 15-year Follow-up. *Am. J. Sports Med.* **2009**, *37*, 688−692.

(2) Sofu, H.; Yildirim, T.; Gursu, S.; Issin, A.; Sahin, V. Short-term Effects of Partial Meniscectomy on the Clinical Results of Anterior Cruciate Ligament Reconstruction. *Knee Surg Sports Traumatol Arthrosc.* **2015**, *23*, 184.

(3) Zantop, T.; Wellmann, M.; Fu, F. H.; Petersen, W. Tunnel Positioning of Anteromedial and Posterolateral Bundles in Anatomic Anterior Cruciate Ligament Reconstruction: Anatomic And Radiographic Findings. *Am. J. Sports Med.* **2008**, *36*, 65−72.

(4) Bourdon-Santoyo, M.; Quinones-Uriostegui, I.; Martinez-Lopez, V.; Sanchez-Arevalo, F.; Alessi-Montero, A.; Velasquillo, C.; Ibarra-Ponce de Leon, C. Preliminary Study of an in Vitro Development of New Tissue Applying Mechanical Stimulation with a Bioreactor as an Alternative for Ligament Reconstruction. *Rev. Invest Clin.* **2014**, *66* (Suppl. 1), S100−S110.

(5) Legnani, C.; Ventura, A.; Terzaghi, C.; Borgo, E.; Albisetti, W. Anterior Cruciate Ligament Reconstruction with Synthetic Grafts. A Review of Literature. *Int. Orthop.* **2010**, *34*, 465−471.

(6) Granan, L. P.; Forssblad, M.; Lind, M.; Engebretsen, L. The Scandinavian ACL Segistries 2004−2007: Baseline Epidemiology. *Acta Orthop.* **2009**, *80*, 563−567.

(7) Ahlden, M.; Kartus, J.; Ejerhed, L.; Karlsson, J.; Sernert, N. Knee Laxity Measurements After Anterior Cruciate Ligament Reconstruction, Using Either Bone-patellar-tendon-bone or Hamstring Tendon Autografts, with Special Emphasis on Comparison over Time. *Knee Surg Sports Traumatol Arthrosc.* **2009**, *17*, 1117−1124.

(8) Karaoglu, S.; Celik, C.; Korkusuz, P. The Effects of Bone Marrow or Periosteum on Tendon-to-bone Tunnel Healing in a Rabbit Model. *Knee Surg Sports Traumatol Arthrosc.* **2009**, *17*, 170−178.

(9) Ichiba, A.; Kishimoto, I. Effects of Articular Cartilage and Meniscus Injuries at The Time of Surgery on Osteoarthritic Changes After Anterior Cruciate Ligament Reconstruction in Patients Under 40 Years Old. *Arch Orthop Trauma Surg.* **2009**, *129*, 409−415.

(10) Mulford, J. S.; Chen, D. Anterior Cruciate Ligament Reconstruction: A Systematic Review of Polyethylene Terephthalate Grafts. *ANZ. J. Surg.* **2011**, *81*, 785−789.

(11) Machotka, Z.; Scarborough, I.; Duncan, W.; Kumar, S.; Perraton, L. Anterior Cruciate Ligament Repair with LARS (Ligament Advanced Reinforcement System): A Systematic Review. *Sports Med. Arthrosc Rehabil Ther Technol.* **2010**, *2*, 29.

(12) Smith, C.; Ajuied, A.; Wong, F.; Norris, M.; Back, D.; Davies, A. The Use of the Ligament Augmentation and Reconstruction System (LARS) for Posterior Cruciate Reconstruction. *Arthroscopy.* **2014**, *30*, 111−120.

(13) Huang, Z.; Bi, L.; Zhang, Z.; Han, Y. Effects of Dimethylolpropionic Acid Modification on the Characteristics of Polyethylene Terephthalate Fibers. *Mol. Med. Rep.* **2012**, *6*, 709−715.

(14) Li, H.; Chen, C.; Ge, Y.; Chen, S. Spray-painted Human Fibronectin Coating as an Effective Strategy to Enhance Graft Ligamentization of a Polyethylene Terephthalate Artificial Ligament. *Biotechnol. Lett.* **2014**, *36*, 1079−1088.

(15) Chollet, C.; Chanseau, C.; Remy, M.; Guignandon, A.; Bareille, R.; Labrugere, C.; Bordenave, L.; Durrieu, M. C. The Effect of RGD Density on Osteoblast and Endothelial Cell Behavior on RGD-grafted Polyethylene Terephthalate Surfaces. *Biomaterials* **2009**, *30*, 711−720.

(16) Chang, T.; Liu, Q.; Marino, V.; Bartold, P. M. Attachment of Periodontal Fibroblasts to Barrier Membranes Coated with Platelet-rich Plasma. *Aust. Dent. J.* **2007**, *52*, 227−233.

(17) Kawai, T.; Yamada, T.; Yasukawa, A.; Koyama, Y.; Muneta, T.; Takakuda, K. Biological Fixation of Fibrous Materials to Bone Using Chitin/chitosan as a Bone Formation Accelerator. *J. Biomed. Mater. Res., Part B* **2009**, *88B*, 264−270.

(18) Murray, M. M.; Spindler, K. P.; Ballard, P.; Welch, T. P.; Zurakowski, D.; Nanney, L. B. Enhanced Histologic Repair in a Central Wound in the Anterior Cruciate Ligament with a Collagen-platelet-rich Plasma Scaffold. *J. Orthop. Res.* **2007**, *25*, 1007−1017.

(19) Vaquette, C.; Viateau, V.; Guerard, S.; Anagnostou, F.; Manassero, M.; Castner, D. G.; Migonney, V. The Effect of Polystyrene Sodium Sulfonate Grafting on Polyethylene Terephthalate Artificial Ligaments on in *Vitro* Mineralisation and in *Vivo* Bone Tissue Integration. *Biomaterials* **2013**, *34*, 7048−7063.

(20) Li, H.; Ge, Y.; Wu, Y.; Jiang, J.; Gao, K.; Zhang, P.; Wu, L.; Chen, S. Hydroxyapatite Coating Enhances Polyethylene Terephthalate Artificial Ligament Graft Osseointegration in the Bone Tunnel. *Int. Orthop.* **2011**, *35*, 1561−1567.

(21) Kurella, A. Review Paper: Surface Modification for Bioimplants: The Role of Laser Surface Engineering. *J. Biomater. Appl.* **2005**, *20*, 5−50.

(22) Lee, C.; Wei, X.; Kysar, J. W.; Hone, J. Measurement of The Elastic Properties and Intrinsic Strength of Monolayer Graphene. *Science* **2008**, *321*, 385−388.

(23) Geim, A. K. Graphene: Status and Prospects. *Science* **2009**, *324*, 1530−1534.

(24) Lee, Y.; Bae, S.; Jang, H.; Jang, S.; Zhu, S. E.; Sim, S. H.; Song, Y. I.; Hong, B. H.; Ahn, J. H. Wafer-scale Synthesis and Transfer of Graphene Films. *Nano Lett.* **2010**, *10*, 490−493.

(25) Sun, X.; Liu, Z.; Welsher, K.; Robinson, J. T.; Goodwin, A.; Zaric, S.; Dai, H. Nano-Graphene Oxide For Cellular Imaging and Drug Delivery. *Nano Res.* **2008**, *1*, 203−212.

(26) Park, J. K.; Jung, J.; Subramaniam, P.; Shah, B. P.; Kim, C.; Lee, J. K.; Cho, J. H.; Lee, C.; Lee, K. B. Graphite-coated Magnetic Nanoparticles as Multimodal Imaging Probes and Cooperative Therapeutic Agents for Tumor Cells. *Small* **2011**, *7*, 1647−1652.

(27) Nayak, T. R.; Andersen, H.; Makam, V. S.; Khaw, C.; Bae, S.; Xu, X.; Ee, P. L.; Ahn, J. H.; Hong, B. H.; Pastorin, G.; Ozyilmaz, B. Graphene for Controlled and Accelerated Osteogenic Differentiation of Human Mesenchymal Stem Cells. *ACS Nano* **2011**, *5*, 4670−4678.

(28) Park, S. Y.; Park, J.; Sim, S. H.; Sung, M. G.; Kim, K. S.; Hong, B. H.; Hong, S. Enhanced Differentiation of Human Neural Stem Cells into Neurons on Graphene. *Adv. Mater.* **2011**, *23*, H263−H267.

(29) Bae, S.; Kim, H.; Lee, Y.; Xu, X.; Park, J. S.; Zheng, Y.; Balakrishnan, J.; Lei, T.; Ri Kim, H.; Song, Y. I.; Kim, Y. J.; Kim, K. S.; Ozyilmaz, B.; Ahn, J. H.; Hong, B. H.; Iijima, S. Roll-to-roll Production of 30-in. Graphene Films for Transparent Electrodes. *Nat. Nanotechnol.* **2010**, *5*, 574−578.

(30) Kim, K. S.; Zhao, Y.; Jang, H.; Lee, S. Y.; Kim, J. M.; Kim, K. S.; Ahn, J. H.; Kim, P.; Choi, J. Y.; Hong, B. H. Large-scale Pattern Growth of Graphene Films for Stretchable Transparent Electrodes. *Nature* **2009**, *457*, 706−710.

(31) Reina, A.; Jia, X.; Ho, J.; Nezich, D.; Son, H.; Bulovic, V.; Dresselhaus, M. S.; Kong, J. Large area, Few-layer Graphene Films on Arbitrary Substrates by Chemical Vapor Deposition. *Nano Lett.* **2009**, *9*, 30−35.

(32) Tsai, S.; Spikings, E.; Kuo, F. W.; Lin, N. C.; Lin, C. Use of an Adenosine Triphosphate Assay, And Simultaneous Staining With Fluorescein Diacetate and Propidium Iodide, To Evaluate the Effects of Cryoprotectants on Hard Coral (Echinopora spp.) Oocytes. *Theriogenology* **2010**, *73*, 605−611.

(33) Gushue, D. L.; Houck, J.; Lerner, A. L. Rabbit Knee Joint Biomechanics: Motion Analysis and Modeling of Forces During Hopping. *J. Orthop. Res.* **2005**, *23*, 735−742.

(34) Foss, C.; Merzari, E.; Migliaresi, C.; Motta, A. Silk Fibroin/hyaluronic Acid 3D Matrices for Cartilage Tissue Engineering. *Biomacromolecules* **2013**, *14*, 38−47.

(35) Li, H.; Ge, Y.; Zhang, P.; Wu, L.; Chen, S. The Effect of Layer-by-layer Chitosan-hyaluronic Acid Coating on Graft-to-bone Healing of a Poly(ethylene terephthalate) Artificial Ligament. *J. Biomater. Sci., Polym. Ed.* **2012**, *23*, 425−438.

(36) Rahaman, M. N.; Mao, J. J. Stem Cell-based Composite Tissue Constructs for Regenerative Medicine. *Biotechnol. Bioeng.* **2005**, *91*, 261−284.

(37) Guidoin, M. F.; Marois, Y.; Bejui, J.; Poddevin, N.; King, M. W.; Guidoin, R. Analysis of Retrieved Polymer Fiber Based Replacements for the ACL. *Biomaterials* **2000**, *21*, 2461−2474.

(38) Lu, B.; Li, T.; Zhao, H.; Li, X.; Gao, C.; Zhang, S.; Xie, E. Graphene-based Composite Materials Beneficial to Wound Healing. *Nanoscale* **2012**, *4*, 2978−2982.

(39) Zong ming, W.; Jian yu, L.; Rui xin, L.; Hao, L.; Yong, G.; Lu, L.; Xin chang, Z.; Xi zheng, Z. Bone Formation in Rabbit Cancellous Bone Explant Culture Model Is Enhanced by Mechanical Load. *Biomed Eng. Online.* **2013**, *12*, 35.

(40) Franceschi, R. T.; Xiao, G. Regulation of the Osteoblast-specific Transcription Factor, Runx2: Responsiveness to Multiple Signal Transduction Pathways. *J. Cell. Biochem.* **2003**, *88*, 446−454.

(41) Jiang, T.; Nukavarapu, S. P.; Deng, M.; Jabbarzadeh, E.; Kofron, M. D.; Doty, S. B.; Abdel-Fattah, W. I.; Laurencin, C. T. Chitosan-poly(lactide-co-glycolide) Microsphere-based Scaffolds for Bone Tissue Engineering: in *Vitro* Degradation and in *Vivo* Bone Regeneration Studies. *Acta Biomater.* **2010**, *6*, 3457−3470.

(42) Salehghaffari, S.; Dhaher, Y. Y. A Model of Articular Cruciate Ligament Reconstructive Surgery: A Validation Construct and Computational Insights. *J. Biomech.* **2014**, *47*, 1609−1617.